Seismic response of a cylindrical tunnel with construction joints subjected to longitudinal ground displacement

Naotoshi Yasuda[a,*], Toshihiro Asakura[b]

[a]*Department of Civil and Earth Resources Engineering, Kyoto University, Katsura, Nishigyou-ku, Kyoto 615-8530, Japan*
[b]*Research group for tunnel engineering, Kajichō, Chiyoda-ku, Tokyo 101-0044, Japan*

Abstract

A seismic response analysis for a mountain tunnel is often two-dimensional, using the tunnel cross-section. However, responses in the longitudinal direction should not be neglected, especially when considering the tunnel lining damage that has been caused by recent earthquakes. A critical factor in the evaluation of the longitudinal seismic response of mountain tunnels is the construction joints, which exist at intervals of approximately 10 m along the lining. In this study, elastic solutions for a cylindrical tunnel with construction joints subjected to longitudinal ground displacement are presented. The surrounding ground is considered to be an infinite elastic, homogeneous, isotropic medium. The lining is treated as an elastic, homogeneous, isotropic medium. The zeroth mode component of an obliquely incident plane harmonic shear wave, which contributes to compression-extension deformation, is used as the longitudinal ground displacement. A no-slip boundary condi-

*corresponding author. Tel.:+81 75 383 7485; Fax: +81 75 383 3218
Email address: yasuda.naotoshi.3x@kyoto-u.ac.jp (Naotoshi Yasuda)

tion is applied at the ground-lining interface, and a traction-free boundary condition is imposed between the interface of the lining blocks. The point-matching method is used to satisfy the boundary conditions at the ground-lining interface approximately. The numerical results show that there is no difference in the seismic response between the case with and the case without the inclusion of construction joints except for the large surface loading in the area neighboring the joints. However, in actuality, the slippage between the ground and the lining can occur and cannot be neglected. Therefore, seismic resistance can be improved by construction joints. When considering slippage, unusually large normal surface loading is required to cause longitudinal seismic damage. Smoothing of the interface between the sheet membrane and the lining, which can also prevent the destruction of the waterproofing membrane and the production and growth of cracks due to drying shrinkage, is an effective countermeasure to prevent the longitudinal seismic damage of mountain tunnels.
Keywords: Mountain tunnel, Seismic response, Elastodynamics, Construction joints, Longitudinal deformation

1. Introduction

It is well known that tunnels experience lower rates of damage than surface structures during earthquake events. Nevertheless, some mountain tunnels have experienced significant damage in recent earthquakes, including the 1995 Kobe (Asakura and Sato, 1996), the 1999 Chi-Chi (Wang et al., 2001; Chen et al., 2002), the 2004 Niigata (Yashiro et al., 2007), the 2008 Wenchuan (Tianbin, 2008; Li, 2012), and the 2016 Kumamoto (Zhang et al.,

2018) events.

Seismic response analyses performed on mountain tunnels are often two-dimensional to evaluate ovaling deformation (Hashash et al., 2005; Kontoe et al., 2008; Amorosi and Boldini, 2009), using only the tunnel cross-section and neglecting the longitudinal direction. However, considering tunnel lining damage caused by recent earthquakes (Wang et al., 2001; Yashiro et al., 2007; Li, 2012; Zhang et al., 2018), responses in the longitudinal direction are also significant. For example, many cracks in the transverse direction of the lining of Tawarayama tunnel were observed to the result from the 2016 Kumamoto earthquake.

The most significant deformation mode for the longitudinal seismic response of mountain tunnels is the compression-extension deformation mode, which causes a large longitudinal thrust loading to be applied to the lining (Yasuda et al., 2019). This deformation mode can cause more severe damage to the lining than ovaling deformation mode, which mainly causes bending deformation, because large thrust can cause sudden compression failure. Recently built tunnels that have been constructed using the New Austrian Tunnelling Method (NATM), including the Tawarayama tunnel, are more prone to damage resulting from this deformation than older tunnels, which were built using prior tunnelling methods. This is due to a decrease in the lining thickness, which resulted in a decreased stiffness for longitudinal thrust. Therefore, the seismic damage caused by large longitudinal thrust loading can increase.

Construction joints, occurring at regular intervals of approximately 10 m along the lining, are a critical factor in the evaluation of the longitudinal seis-

mic response of mountain tunnels. It is expected that construction joints improve earthquake resistance because flexible joints are used in buried pipelines and immersed tunnels to enhance earthquake resistance (Kiyomiya, 1995; O'Rourke and Liu, 1999; Shi, 2015). In Tawarayama tunnel, the construction joints seemed to have some effects on the damage incurred from the 2016 Kumamoto earthquake as ring cracks occurred in the middle of the lining blocks approximately every 10 m (Zhang et al., 2018). However, theoretical explanations behind this phenomenon, especially the seismic behavior of construction joints, are not clear.

Simplified models such as beam on elastic foundation model and beam-spring model are usually used for the seismic design of tunnels in the longitudinal direction (St John and Zahrah, 1987; Hashash et al., 2001; Miao et al., 2018; Yu et al., 2018). However, these models are not suitable for problems with the sudden change of properties. It is because the stiffness of the ground model, which is often modeled as a constant spring, does not change against sudden deformation, although the stiffness of the structure model increases against sudden deformation. Therefore, it is difficult to evaluate the effect of joints strictly. Three-dimensional numerical models, such as the Boundary Element Method and the Finite Element Method, can also be used (Stamos and Beskos, 1995; Fabozzi et al., 2018; Wang et al., 2019). However, they are highly time-consuming and need huge computer memory. Besides, they are also not suitable for problems with the sudden change of properties. The multi-scale method (Yu et al., 2013) is one of the leading solutions. Nevertheless, it is still difficult to apply this study because there are many joints to be considered, which need very fine-scale meshes.

This paper presents elastic solutions for a cylindrical tunnel with construction joints subjected to longitudinal ground displacement, which contributes to compression-extension deformation. The solutions are derived using the substructure method (Wolf, 1985) and the point-matching method (Yasuda et al., 2017). The effects of construction joints are strictly investigated. Furthermore, a possible countermeasure against longitudinal seismic damage in the linings is proposed.

2. Theory

2.1. Problem definition

Consider an infinite cylindrical tunnel with construction joints subjected to a plane harmonic shear wave propagating at an angle ϕ with respect to the axis of the cylindrical tunnel, as shown in Fig. A.1. The surrounding ground is considered to be an infinite elastic, homogeneous, isotropic medium. The lining is treated as an elastic, homogeneous, isotropic medium with an outer radius R and a thickness h. The layer of the sprayed concrete is not considered. The interval between construction joints is ℓ. The local coordinate in the z-direction in the pth lining block is z_p.

Due to the azimuthal symmetry of the circular cylinder, an incident shear wave can be assumed to propagate in the direction of the wavenumber vector $\boldsymbol{k}_{s(1)}^{\mathrm{inc}}$ on the x-z plane; superscript " inc " denotes an incident wave and subscript (1) denotes the ground. The angular velocity of the incident shear wave is ω. The displacement vector of the shear wave $\boldsymbol{u}_{s(1)}^{\mathrm{inc}}$ is on the plane perpendicular to $\boldsymbol{k}_{s(1)}^{\mathrm{inc}}$ and can be decomposed into two independent vectors: One is parallel to the y-axis and the other is on the x-z plane. Here, only

the seismic response resulting from a longitudinal ground displacement (displacement in the z-direction) is considered. Therefore, $\boldsymbol{u}_{s(1)}^{\mathrm{inc}}$ is assumed to be on the x-z plane.

To derive the theoretical solutions, periodic boundary conditions are assumed in the longitudinal direction with an interval length of L_z. This interval length equals the longitudinal wavelength and can be expressed as:

$$L_z = \frac{L_{s(1)}}{\cos\phi}, \tag{1}$$

where $L_{s(1)}$ is the wavelength of an incident ground shear wave.

2.2. The zeroth mode component of the incident shear wave

The x- and z- components of the incident harmonic shear wave $\boldsymbol{u}_{\mathrm{s(1)}}^{\mathrm{inc}}$ can be expressed as:

$$\left.\begin{aligned} u_{x(1)}^{\mathrm{inc}} &= U_{x(1)}^{\mathrm{inc}} e^{i\left(\boldsymbol{k}_{s(1)}^{\mathrm{inc}}\cdot\boldsymbol{r}-\omega t\right)} \\ &= U_{s(1)}^{\mathrm{inc}}\cos\phi e^{i(\beta_{(1)}x+\gamma z-\omega t)} \\ u_{z(1)}^{\mathrm{inc}} &= U_{z(1)}^{\mathrm{inc}} e^{i\left(\boldsymbol{k}_{s(1)}^{\mathrm{inc}}\cdot\boldsymbol{r}-\omega t\right)} \\ &= -U_{s(1)}^{\mathrm{inc}}\sin\phi e^{i(\beta_{(1)}x+\gamma z-\omega t)} \end{aligned}\right\}, \tag{2}$$

with:

$$\left.\begin{aligned} k_{s(1)} &= \frac{2\pi}{L_s} \\ \beta_{(1)} &= k_{s(1)}\sin\phi \\ \gamma &= k_{s(1)}\cos\phi = \frac{2\pi}{L_z} \end{aligned}\right\}, \tag{3}$$

where $U_{s(1)}^{\mathrm{inc}}$ is the complex displacement amplitude of the incident shear wave and $U_{x(1)}^{\mathrm{inc}}$ and $U_{z(1)}^{\mathrm{inc}}$ are the x- and z- components of $U_{s(1)}^{\mathrm{inc}}$, respectively. $\boldsymbol{r}$ is

the position vector. $k_{s(1)}$ is the shear wavenumber in the ground and $\beta_{(1)}$ and γ are the x-axis and z-axis components of $k_{s(1)}$, respectively.

The exponential function $e^{i\beta_{(1)}x}$ can be expanded into a Fourier series in its complex form, or

$$e^{i\beta_{(1)}x} = e^{i\beta_{(1)}r\cos\theta} = \sum_{n=-\infty}^{\infty} i^n J_n(\beta_{(1)}r)e^{in\theta}, \tag{4}$$

where J_n denotes the Bessel functions of the first kind, order n. From Eq. (2) to (4), the r-, θ-, and z- components of the incident harmonic shear wave $\boldsymbol{u}_{s(1)}^{\text{inc}}$ are given by:

$$\left.\begin{aligned} u_{r(1)}^{\text{inc}} &= \quad U_{s(1)}^{\text{inc}}\cos\phi\cos\theta \sum_{n=-\infty}^{\infty} i^n J_n(\beta_{(1)}r)e^{in\theta}e^{i(\gamma z-\omega t)} \\ u_{\theta(1)}^{\text{inc}} &= -U_{s(1)}^{\text{inc}}\cos\phi\sin\theta \sum_{n=-\infty}^{\infty} i^n J_n(\beta_{(1)}r)e^{in\theta}e^{i(\gamma z-\omega t)} \\ u_{z(1)}^{\text{inc}} &= -U_{s(1)}^{\text{inc}}\sin\phi \sum_{n=-\infty}^{\infty} i^n J_n(\beta_{(1)}r)e^{in\theta}e^{i(\gamma z-\omega t)} \end{aligned}\right\}. \tag{5}$$

The zeroth mode component of the incident shear wave, which is independent of θ and represents the compression-extension deformation, at the ground-lining interface with $r = R$ can be expressed as:

$$\left.\begin{aligned} u_{r,0(1)}^{\text{inc}}|_{r=R} &= \quad U_{s(1)}^{\text{inc}}\cos\phi i J_1(\beta_{(1)}R)e^{i(\gamma z-\omega t)} \\ u_{\theta,0(1)}^{\text{inc}}|_{r=R} &= \quad 0 \\ u_{z,0(1)}^{\text{inc}}|_{r=R} &= -U_{s(1)}^{\text{inc}}\sin\phi J_0(\beta_{(1)}R)e^{i(\gamma z-\omega t)} \end{aligned}\right\}, \tag{6}$$

where the subscript 0 denotes the zeroth mode component.

In general, the wavelength of seismic shear wave is sufficiently greater than the size of the tunnel cavity. Therefore, $\beta_{(1)}R$ is much less than 1.

Considering a series expansion of $J_n(x)$ around $x = 0$ as follow:

$$J_n(x) = \sum_{s=0}^{\infty} \frac{(-1)^s}{s!(n+s)!} \left(\frac{x}{2}\right)^{n+2s}, \tag{7}$$

the relative amplitudes of $u^{\text{inc}}_{r,0(1)}$ and $u^{\text{inc}}_{z,0(1)}$ can be approximately expressed as:

$$\left.\begin{aligned} \left|\frac{u^{\text{inc}}_{r,0(1)}}{u^{\text{inc}}_{x(1)}}\right|_{r=R} &\approx \frac{\beta_{(1)}R}{2} \\ \left|\frac{u^{\text{inc}}_{z,0(1)}}{u^{\text{inc}}_{z(1)}}\right|_{r=R} &\approx 1 - \left(\frac{\beta_{(1)}R}{2}\right)^2 \end{aligned}\right\}. \tag{8}$$

Thus, almost all longitudinal ground displacement of the incident shear wave contributes to the zeroth mode component. In the following section, the seismic response caused by the zeroth mode component of the incident shear wave is considered.

2.3. General solutions for the ground and lining

2.3.1. Solution for the primary field of the ground

When a plane harmonic shear wave impinges on a surface of a ground cavity with no lining, part of the incident wave is reflected at the cavity. The primary displacement of the ground for the zeroth mode component $\boldsymbol{u}^i_{0(1)}$, which is the superposition of an incident wave of the zeroth component $\boldsymbol{u}^{\text{inc}}_{0(1)}$ and the reflected wave, can be calculated using elastodynamics (Mow and Pao, 1971). At the ground-lining interface with $r = R$, $\boldsymbol{u}^i_{0(1)}$ can be expressed as follows:

$$\left.\begin{aligned} u^i_{r,0(1)}|_{r=R} &= U^i_{r,0(1)} e^{i(\gamma z - \omega t)} \\ u^i_{z,0(1)}|_{r=R} &= U^i_{z,0(1)} e^{i(\gamma z - \omega t)} \end{aligned}\right\}, \tag{9}$$

where $U^i_{r,0(1)}$ and $U^i_{z,0(1)}$ are complex constants. The superscript i is used to denote initiation.

2.3.2. Solution for the secondary field of the ground

Displacement and surface loading of the ground caused by the reflected wave at the ground-lining interface can be expressed as follows:

$$\left.\begin{aligned} u^r_{r,0(1)}|_{r=R} &= \sum_{m=0}^{\infty}\left(U^r_{r,0m(1)}e^{i\gamma_m z} + U'^{,r}_{r,0m(1)}e^{-i\gamma_m z}\right)e^{-i\omega t} \\ u^r_{z,0(1)}|_{r=R} &= \sum_{m=0}^{\infty}\left(U^r_{z,0m(1)}e^{i\gamma_m z} + U'^{,r}_{z,0m(1)}e^{-i\gamma_m z}\right)e^{-i\omega t} \end{aligned}\right\}, \tag{10}$$

$$\left.\begin{aligned} f^r_{r,0(1)} = -\sigma_{rr,0(1)}|_{r=R} &= \sum_{m=0}^{\infty}\left(F^r_{r,0m(1)}e^{i\gamma_m z} + F'^{,r}_{r,0m(1)}e^{-i\gamma_m z}\right)e^{-i\omega t} \\ f^r_{z,0(1)} = -\sigma_{rz,0(1)}|_{r=R} &= \sum_{m=0}^{\infty}\left(F^r_{z,0m(1)}e^{i\gamma_m z} + F'^{,r}_{z,0m(1)}e^{-i\gamma_m z}\right)e^{-i\omega t} \end{aligned}\right\}, \tag{11}$$

with:

$$\gamma_m = \frac{2\pi m}{L_z}, \tag{12}$$

where $U^r_{r,0m(1)}$, $U'^{,r}_{r,0m(1)}$, and so on are complex constants, and $U'^{,r}_{r,00(1)}$, $U'^{,r}_{z,00(1)}$, $F'^{,r}_{r,00(1)}$, and $F'^{,r}_{z,00(1)}$ are assumed to be zero. The superscript r is used to denote reaction.

The stiffness of the ground, which is defined as the relationship between displacement and surface loading at the ground-lining interface, for the zeroth mode can be defined as follows (Yasuda et al., 2017, 2019):

$$\begin{pmatrix} F^r_{r,0m(1)} \\ F^r_{z,0m(1)} \end{pmatrix} = \begin{pmatrix} K_{rr,0m(1)} & K_{rz,0m(1)} \\ -K_{rz,0m(1)} & K_{zz,0m(1)} \end{pmatrix} \begin{pmatrix} U^r_{r,0m(1)} \\ U^r_{z,0m(1)} \end{pmatrix}, \tag{13}$$

$$\begin{pmatrix} F'^{,r}_{r,0m(1)} \\ F'^{,r}_{z,0m(1)} \end{pmatrix} = \begin{pmatrix} K_{rr,0m(1)} & -K_{rz,0m(1)} \\ K_{rz,0m(1)} & K_{zz,0m(1)} \end{pmatrix} \begin{pmatrix} U'^{,r}_{r,0m(1)} \\ U'^{,r}_{z,0m(1)} \end{pmatrix}, \tag{14}$$

and

$$\left.\begin{aligned} K_{rr,0m(1)} &= \frac{2\mu_{(1)}}{R\Delta}\left(-\frac{k^2_{s(1)}\beta_{m(1)}R}{2}h_{00} + \gamma_m^2 h_{01} + \alpha_{m(1)}\beta_{m(1)}h_{10}\right) \\ K_{rz,0m(1)} &= i\frac{2\mu_{(1)}\gamma_m}{\Delta}\left\{ -\frac{1}{2}(\beta^2_{m(1)} - \gamma_m^2)h_{01} + \alpha_{m(1)}\beta_{m(1)}h_{10}\right\} \\ K_{zz,0m(1)} &= \frac{\mu_{(1)}\alpha_{m(1)}k^2_{s(1)}}{\Delta}h_{11} \end{aligned}\right\}, \tag{15}$$

with:

$$\left.\begin{aligned} \Delta &= \gamma_m^2 h_{01} + \alpha_{m(1)}\beta_{m(1)}h_{10} \\ h_{ij} &= H_i^{(1)}(\alpha_{m(1)}R)H_j^{(1)}(\beta_{m(1)}R) \\ \alpha_{m(1)} &= \sqrt{k^2_{p(1)} - \gamma_m^2} \\ \beta_{m(1)} &= \sqrt{k^2_{s(1)} - \gamma_m^2} \end{aligned}\right\}, \tag{16}$$

where $\mu_{(1)}$ is the shear modulus of the ground and $k_{p(1)}$ is the pressure wavenumber in the ground. $H_n^{(1)}$ denotes the Hankel functions of the first order n.

2.3.3. Solutions for the lining

Here, for simplicity, the lining is treated as an elastic cylindrical shell, with thickness h being considerably smaller than the outer radius of the lining R. Therefore, the mean radius of the shell is considered to be equal to R. The total number of lining blocks in the interval L_z is assumed to be P.

The general solutions of the pth lining blocks at the ground-lining interface with $r = R$ can be expressed as follows:

$$\left.\begin{aligned} u_{r,0(2\text{-}p)} &= \sum_{n=0}^{\infty} \left(U_{r,0n(2\text{-}p)} e^{i\Gamma_n z_p} + U'_{r,0n(2\text{-}p)} e^{-i\Gamma_n z_p} \right) e^{-i\omega t} \\ u_{z,0(2\text{-}p)} &= \sum_{n=0}^{\infty} \left(U_{z,0n(2\text{-}p)} e^{i\Gamma_n z_p} + U'_{z,0n(2\text{-}p)} e^{-i\Gamma_n z_p} \right) e^{-i\omega t} \end{aligned}\right\}, \tag{17}$$

$$\left.\begin{aligned} f_{r,0(2\text{-}p)} &= \sum_{n=0}^{\infty} \left(F_{r,0n(2\text{-}p)} e^{i\Gamma_n z_p} + F'_{r,0n(2\text{-}p)} e^{-i\Gamma_n z_p} \right) e^{-i\omega t} \\ f_{z,0(2\text{-}p)} &= \sum_{n=0}^{\infty} \left(F_{z,0n(2\text{-}p)} e^{i\Gamma_n z_p} + F'_{z,0n(2\text{-}p)} e^{-i\Gamma_n z_p} \right) e^{-i\omega t} \end{aligned}\right\}, \tag{18}$$

with:

$$\Gamma_n = \frac{\pi n}{\ell}, \tag{19}$$

where $U_{r,0n(2\text{-}p)}$, $U'_{r,0n(2\text{-}p)}$, and so on are complex constants, and $U'_{r,00(2\text{-}p)}$, $U'_{z,00(2\text{-}p)}$, $F'_{r,00(2\text{-}p)}$, and $F'_{z,00(2\text{-}p)}$ are assumed to be zero. The subscript (2-p) denotes the pth lining block.

The relationships between displacement and loading for the zeroth mode can be derived from Eq. (17), Eq. (18), and the relationship between the displacement and the load acting on the shell (Flügge, 1973). They can be expressed as follows:

$$\begin{pmatrix} F_{r,0n(2\text{-}p)} \\ F_{z,0n(2\text{-}p)} \end{pmatrix} = \begin{pmatrix} K_{rr,0n(2)} & K_{rz,0n(2)} \\ -K_{rz,0n(2)} & K_{zz,0n(2)} \end{pmatrix} \begin{pmatrix} U_{r,0n(2\text{-}p)} \\ U_{z,0n(2\text{-}p)} \end{pmatrix}, \tag{20}$$

$$\begin{pmatrix} F'_{r,0n(2\text{-}p)} \\ F'_{z,0n(2\text{-}p)} \end{pmatrix} = \begin{pmatrix} K_{rr,0n(2)} & -K_{rz,0n(2)} \\ K_{rz,0n(2)} & K_{zz,0n(2)} \end{pmatrix} \begin{pmatrix} U'_{r,0n(2\text{-}p)} \\ U'_{z,0n(2\text{-}p)} \end{pmatrix}, \tag{21}$$

where

$$\left.\begin{aligned} K_{rr,0n(2)} &= \frac{D}{R^2} + \frac{K}{R^4}\{1 + (\Gamma_n R)^4\} \\ K_{rz,0n(2)} &= i\Gamma_n R \left\{ \frac{D}{R^2}\nu_{(2)} + \frac{K}{R^4}(\Gamma_n R)^2 \right\} \\ K_{zz,0n(2)} &= \frac{D}{R^2}(\Gamma_n R)^2 \end{aligned}\right\}, \tag{22}$$

with:

$$\left.\begin{aligned} D &= \frac{E_{(2)}h}{1-\nu_{(2)}^2} \\ K &= \frac{E_{(2)}h^3}{12\left(1-\nu_{(2)}^2\right)} \end{aligned}\right\}, \tag{23}$$

where D is the extensional rigidity and K is the flexural rigidity. $E_{(2)}$ and $\nu_{(2)}$ are the Young's modulus and Poisson's ratio of the lining, respectively.

The axial thrust and bending moment can be calculated from the displacement of the lining as expressed below:

$$\left.\begin{aligned} n_{zz,0(2\text{-}p)} &= \sum_{n=0}^{\infty} \left(N_{zz,0n(2\text{-}p)} e^{i\Gamma_n z_p} + N'_{zz,0n(2\text{-}p)} e^{-i\Gamma_n z_p} \right) e^{-i\omega t} \\ m_{zz,0(2\text{-}p)} &= \sum_{n=0}^{\infty} \left(M_{zz,0n(2\text{-}p)} e^{i\Gamma_n z_p} + M'_{zz,0n(2\text{-}p)} e^{-i\Gamma_n z_p} \right) e^{-i\omega t} \end{aligned}\right\}, \tag{24}$$

where $N_{zz,0n(2\text{-}p)}$, $N'_{zz,0n(2\text{-}p)}$, $M_{zz,0n(2\text{-}p)}$, and $M'_{zz,0n(2\text{-}p)}$ are complex constants. These constants can be determined as:

$$\begin{pmatrix} N_{zz,0n(2\text{-}p)} \\ M_{zz,0n(2\text{-}p)} \end{pmatrix} = \begin{pmatrix} K_{Nr,0n(2)} & K_{Nz,0n(2)} \\ K_{Mr,0n(2)} & K_{Mz,0n(2)} \end{pmatrix} \begin{pmatrix} U_{r,0n(2\text{-}p)} \\ U_{z,0n(2\text{-}p)} \end{pmatrix}, \tag{25}$$

$$\begin{pmatrix} N'_{zz,0n(2\text{-}p)} \\ M'_{zz,0n(2\text{-}p)} \end{pmatrix} = \begin{pmatrix} K_{Nr,0n(2)} & -K_{Nz,0n(2)} \\ K_{Mr,0n(2)} & -K_{Mz,0n(2)} \end{pmatrix} \begin{pmatrix} U'_{r,0n(2\text{-}p)} \\ U'_{z,0n(2\text{-}p)} \end{pmatrix}, \tag{26}$$

where

$$\left.\begin{aligned} K_{Nr,0n(2)} &= \frac{D}{R}\nu_{(2)} + \frac{K}{R^3}(\Gamma_n R)^2 \\ K_{Nz,0n(2)} &= i\frac{D}{R}(\Gamma_n R) \\ K_{Mr,0n(2)} &= -\frac{K}{R^2}(\Gamma_n R)^2 \\ K_{Mz,0n(2)} &= -i\frac{K}{R^2}(\Gamma_n R) \end{aligned}\right\}. \tag{27}$$

The longitudinal axial stress of the pth lining $\sigma_{zz,0(2\text{-}p)}$ can be approximately calculated from $n_{zz,0(2\text{-}p)}$ and $m_{zz,0(2\text{-}p)}$ as follows:

$$\sigma_{zz,0(2\text{-}p)} \approx \frac{1}{h - \frac{I}{R^2}} \left\{ \left(1 \pm \frac{h}{2R}\right) n_{zz,0(2\text{-}p)} + \left(\pm\frac{h^2}{2I} + \frac{1}{R}\right) m_{zz,0(2\text{-}p)} \right\}, \tag{28}$$

with:

$$I = \frac{h^3}{12}, \tag{29}$$

where I is the moment of inertia of the lining. As for $\pm$ in Eq. (28), the positive and negative signs are chosen for the inner and outer surfaces of the lining, respectively.

2.4. Solution under ground-lining interaction

2.4.1. Boundary conditions

A no-slip boundary condition is applied at the ground-lining interface with $r = R$ as follows:

$$\left.\begin{aligned} u^i_{r,0(1)}|_{r=R} + u^r_{r,0(1)}|_{r=R} &= u_{r,0(2\text{-}p)}|_{r=R} \\ u^i_{z,0(1)}|_{r=R} + u^r_{z,0(1)}|_{r=R} &= u_{z,0(2\text{-}p)}|_{r=R} \\ f_{r,0(1)}|_{r=R} + f_{r,0(2\text{-}p)}|_{r=R} &= 0 \\ f_{z,0(1)}|_{r=R} + f_{z,0(2\text{-}p)}|_{r=R} &= 0 \end{aligned}\right\}. \tag{30}$$

A traction-free boundary condition is imposed between the interface of the lining blocks as follows:

$$\left.\begin{aligned} n_{zz,0(2\text{-}p)}\big|_{z_p=\pm\frac{\ell}{2}} &= 0 \\ m_{zz,0(2\text{-}p)}\big|_{z_p=\pm\frac{\ell}{2}} &= 0 \end{aligned}\right\}. \tag{31}$$

2.4.2. Point matching method

When there is no construction joint in the lining, only the no-slip condition at the ground–lining interface is imposed, and the boundary condition can be strictly satisfied. However, it is impossible to satisfy the boundary conditions when there are joints. Therefore, the point matching method, where the conditions are satisfied only at a finite set of selected points, is adopted. For imposing the no-slip boundary condition, Q equidistantly spaced points are selected in every lining block ($z_{p,q} = \ell(-Q-1+2q)/(2Q+2)$). Thus, a total of PQ points are selected in the ground. The traction-free boundary condition is imposed at both ends of the lining ($z_p = \pm\ell/2$). When both P and Q are odd numbers, the first $(PQ+1)/2$ terms of m (from $m=0$ to $(PQ-1)/2$) and $(Q+3)/2$ terms of n (from $n=0$ to $(Q+1)/2$) are used to represent the approximate solutions. The resulting system of inhomogeneous linear equations is solved by matrix inversion, which was performed with quadruple precision to prevent the cancellation of significant digits.

3. Results and discussion

For the sample numerical calculations, the Shinkansen tunnel in soft ground was considered due to the severe earthquake damage observed in tunnels covered by soft ground. Table. A.1 lists the material properties used

for the numerical calculations. The ratio of Young's modulus of the ground and the lining is 0.01:1. The shear wave velocity in the ground is approximately 240 m/s. The tunnel is assumed to be constructed using NATM, and the secondary lining is only considered. The amplitude of the incident shear wave displacement $\boldsymbol{u}^{\mathrm{inc}}_{s(1)}$ is assumed to be 10 mm.

3.1. Solutions with no construction joint

The case with no joints is first investigated to understand the basic seismic response. In this case, the lining length ℓ becomes equal to the longitudinal wavelength of the incident shear wave L_z, and only the first mode ($m = n = 1$) is contained in the solution.

Fig. A.2 shows the longitudinal displacements at the ground-lining interface $r = R$. The frequency f of the incident shear wave is 1.0 Hz. There is little difference between the longitudinal ground displacement of the incident shear wave $u^{\mathrm{inc}}_{z(1)}$ and that of the primary field of the zeroth mode component $u^{i}_{z,0(1)}$, which is the superposition of an incident wave and the reflected wave from a ground cavity. This means that the presence of the cavity has little effect on the longitudinal ground displacement when the frequency is low. The longitudinal displacement of the lining $u_{z,0(2)}$ is smaller than $u^{i}_{z,0(1)}$. The amplitude ratio of $u_{z,0(2)}$ to $u^{i}_{z,0(1)}$ is approximately 0.73 at an incident angle of 45° and increases with increasing ϕ. This is mainly because the wavelength along the tunnel axis L_z increases with increasing ϕ, and the stiffness of the lining decreases with increasing L_z as shown in Eq. (22). It should be noted that singular behavior is observed at an incident angle of approximately 60°. It is because $\alpha_{1(1)}$ in Eq. (16) approaches to zero. As the longitudinal wavelength L_z approaches to the wavelength of ground pressure wave $L_{p(1)}$, the

phase of the reflected waves excited at the ground-lining interface matches well. As a result, a kind of resonance is excited, and the stiffness of the ground is suddenly decreased.

Fig. A.3 shows the longitudinal displacements at the ground-lining interface. The frequency is 5.0 Hz. In this case, there is some difference between $u^{\mathrm{inc}}_{z(1)}$ and $u^{i}_{z,0(1)}$. This means that the presence of the cavity causes some effect on the longitudinal ground displacement when the frequency is high. The amplitude ratio of $u_{z,0(2)}$ to $u^{i}_{z,0(1)}$ is approximately 0.18 at an incident angle of 45° and decreases at all incident angles as compared to that for 1.0 Hz. This is mainly a result of the stiffness of the lining, increasing with decreasing L_z.

Fig. A.4 shows the surface loadings and longitudinal axial stress at the middle surfaces of the lining. The frequency f is 1.0 Hz. The phase of $u_{z,0(2)}$, which is shown in Fig. A.2, and $f_{z,0(2)}$ are close. In contrast to this, the phase of $f_{z,0(2)}$ and $\sigma_{zz,0(2)}$ differs by a quarter wavelength. The amplitude of $\sigma_{zz,0(2)}$ is much larger than that of $f_{r,0(2)}$ or $f_{z,0(2)}$. At an incident angle of 45°, the amplitude of $\sigma_{zz,0(2)}$ is approximately 180 times larger than that of $f_{z,0(2)}$. This is a result of $\sigma_{zz,0(2)}$ being approximately consistent with the accumulation of $f_{z,0(2)}$ in the longitudinal direction. $\sigma_{zz,0(2)}$ becomes a maximum at an incident angle of approximately 50°. It should be noted that $\sigma_{zz,0(2)}$ becomes a maximum at an incident angle of 45° when the tunnel is sufficiently flexible relative to the surrounding ground and completely follows the ground deformation.

Fig. A.5 shows the surface loadings and longitudinal axial stress at the middle surfaces of the lining. The frequency f is 5.0 Hz. The amplitude of

$\sigma_{zz,0(2)}$ is still much larger than that of $f_{r,0(2)}$ or $f_{z,0(2)}$. However, the amplitude ratio of $\sigma_{zz,0(2)}$ to $f_{z,0(2)}$ is smaller than that found for a frequency of 1.0 Hz. At an incident angle of 45°, the amplitude of $\sigma_{zz,0(2)}$ is approximately 36 times larger than that of $f_{z,0(2)}$. $\sigma_{zz,0(2)}$ is a maximum at an incident angle of approximately 70° as the result of the ground-lining interaction.

3.2. Solution with the inclusion of construction joints

In the following sample case solution, the interval between construction joints ℓ and the number of the lining blocks P are assumed to be 10 m and 35, respectively. As a result, the longitudinal wavelength of the incident wave L_z is 350 m. When the frequency f is 1.0 Hz, the incident angle is approximately 47°.

Fig. A.6 shows approximate solutions for the longitudinal axial stress at the middle lining surface. The frequency f is 1.0 Hz. Q equidistantly spaced points were selected in every lining block for imposing the non-slip condition. The approximate solutions become more accurate with increasing Q with the solution converging to the solution without construction joints, except for around the joints. This means there is only a minor difference in the longitudinal axial stress between the case with and the case without the inclusion of construction joints.

Fig. A.7 shows a comparison of the solutions for the case with and without construction joints. The non-slip condition was applied at 71 selected points in every 10 m lining block (Q=71). The displacements are mostly similar to the two cases. However, a large difference in surface loading can be observed. The surface shear loading $f_{z,0(2)}$ in the area neighboring the joints is especially large. The ends are singular points with the loading approaching infinity

as the degree of freedom increases. When neglecting slippage between the ground and the lining, there is little difference in seismic response between the case with and the case without construction joints. However, in actuality, the slippage can occur and cannot be neglected. The construction joints induce the large surface shear loading in the area neighboring the joints. As a result, the slippage is induced more easily, and the seismic resistance can be improved.

Fig. A.8 shows solutions derived from a simplified model assuming a constant ground stiffness. Details of the solution are shown in Appendix A. The subscript (2s) denotes the solution of the simplified model. For longitudinal axial stress $\sigma_{zz,0(2s)}$, the value multiplied by ten is plotted. When there is no construction joint, the simplified model can well evaluate the solutions. When there are construction joints, $\sigma_{zz,0(2s)}$ becomes almost zero. Assuming the result is correct, it is difficult to explain the cracks in the transverse direction of the lining that occurred during past earthquakes. This is because the stiffness of the ground around joints does not change, although the stiffness of the tunnel around joints increases. Therefore, the model assuming a constant ground stiffness overestimate the effect of construction joints and is not suitable.

3.3. Relationship between the applied surface loading and the resulting axial stress in the lining

To discuss the effects of construction joints in detail, it is necessary to consider the slippage. Recent tunnels, including the Tawarayama tunnel, have a sprayed concrete layer between the ground and the tunnel lining. Additionally, a sheet membrane with a geotextile fleece is placed between the

sprayed concrete layer and the lining. For simplification, only the relationship between the surface shear loading and the resulting longitudinal axial stress in the lining is herein considered.

Fig. A.9 shows the applied surface loading $f_{z,0(2)}$ and the resulting longitudinal axial stress at the middle surfaces of the lining. $f_{r,0(2)}$ is assumed to be zero for simplicity because $f_{r,0(2)}$ has little effect on the longitudinal axial stress. Furthermore, the surface shear loading $f_{z,0(2)}$ is assumed to be zero at the center of the lining block and monotonically increases or decreases towards the edge. The maximum allowable surface shear loading is assumed to be 0.2 MPa. A surface shear loading of approximately 0.2 MPa is required to cause tensile cracks in the lining for an assumed concrete tensile strength of 2.0 MPa. It should be noted that the effect of construction joints can be ignored for the compression side, and the required surface shear loading for the compressive failure of the lining is approximately the same magnitude as compared to that required to cause tensile cracks, as predicted from Fig. A.4 and Fig. A.5.

A result of a shear test, which was performed in the laboratory to investigate the load-shearing effects between the sheet membrane with a geotextile fleece and the lining, shows that Coulomb's law of friction is valid and applicable, and the shear angle is approximately 16.5 degrees (Galler and Lorenz, 2018). This means that the allowable surface shear loading to the lining depends on the surface normal loading. Furthermore, the normal loading required for a shear loading of more than 0.2 MPa in the lining is approximately 0.7 MPa. This is equivalent to an approximately 30 m overburden and means unusually large normal surface loading is required to cause tensile cracks in

the lining.

For actual tunnels, there are likely more irregularities in their construction than assumed in a laboratory test. Therefore, longitudinal seismic damage would occur at much less than 0.7 MPa. Nonetheless, a large normal loading is required to cause longitudinal seismic damage and such damage rarely occurs.

Recently, the Shinkansen tunnel in Japan is required to apply the Flat Insulated Lining Method, which adds a layer between the sheet membrane and the lining to eliminate the unexpected significant irregularities that often occur in actual tunnels. This method is for preventing the waterproofing membrane destruction and the production and growth of cracks due to drying shrinkage. Although this method was not developed for improving seismic resistance, it can reduce the shear loading acting on the lining. Such a smoothing of the interface is an effective countermeasure to prevent the longitudinal seismic damage of tunnels. Besides, it can also improve the seismic resistance in the transverse direction of tunnels (Sedarat et al., 2009). It should be noted that the isolation layer, which is a method to cover a tunnel lining with a soft and thin coating (Kim and Konagai, 2000; Chen and Shen, 2014), is not suitable for mountain tunnel because it can loosen the surrounding ground, which can apply the large loading on the lining before an earthquake.

4. Conclusions

The elastic solutions for a cylindrical tunnel with construction joints subjected to longitudinal ground displacement were presented. The effects of

construction joints were investigated with a countermeasure against the longitudinal seismic damage. The following conclusions can be drawn from this study:

(1) There is no difference in the seismic response between the case with and the case without the inclusion of construction joints except for the large surface loading induced in the area neighboring the joints when considering the interaction between the tunnel and the surrounding ground strictly with the no-slip condition.

(2) The model assuming a constant ground stiffness is not suitable for evaluating the effect of construction joints. This is because the stiffness of the ground does not change around the joints although the stiffness of the tunnel increases around the joints.

(3) When considering the slippage, seismic resistance is improved by construction joints because the slippage is induced by the large surface shear loading in the area neighboring the joints.

(4) When the shear angle between the sheet membrane and the lining is equal to that obtained from the laboratory tests, unusually large normal surface loading is required to cause longitudinal seismic damage. Therefore, longitudinal seismic damage rarely occurs.

(5) Smoothing of the interface to reduce the shear loading acting on the lining, which is usually applied for preventing the destruction of the waterproofing membrane and the production and growth of cracks due

to drying shrinkage, is an effective countermeasure to prevent the longitudinal seismic damage of mountain tunnels.

Appendix A. Solutions of simplified model assuming a constant ground stiffness

The governing equation of the simplified model, in which lining is assumed as a rod and the surrounding ground is assumed as a constant stiffness, is given by (St John and Zahrah, 1987):

$$-E_{(2)}A_c\frac{d^2u_{z,0(2s)}}{dz^2} = K_a\left(u_{z,0(1)} - u_{z,0(2s)}\right)\left(= f_{z,0(2s)}\right), \tag{A.1}$$

where $E_{(2)}$, A_c, and $u_{z,0(2s)}$ are the Young's modulus, the cross-sectional area, and the longitudinal displacement of the lining, respectively. A constant K_a is a complex constant, and $u_{z,0(1)}$ is the longitudinal displacement of the ground. The validity of this model has been confirmed based on elastodynamics and shell theory (Yasuda et al., 2014), and parameter A_c, K_a and $u_{z,0(1)}$ can be expressed as follows:

$$A_c = 2\pi Rh, \tag{A.2}$$

$$K_a = 2\pi RK_{zz,01(1)}, \tag{A.3}$$

$$u_{z,0(1)} = u^i_{z,0(1)}|_{r=R} = U^i_{z,0(1)}e^{i(\gamma z-\omega t)}, \tag{A.4}$$

where R and h are mean radius and thickness of the lining, respectively. $u^i_{z,0(1)}|_{r=R}$ and $K_{zz,01(1)}$ are defined by Eq. (9) and Eq. (15).

When the lining is infinite and there is no construction joint, the solution of Eq. (A.1) can be expressed as follows:

$$u_{z,0(2s)} = \frac{\lambda^2}{\lambda^2+\gamma^2}U^i_{z,0(1)}e^{i(\gamma z-\omega t)}, \tag{A.5}$$

with:

$$\lambda^2 = \frac{K_a}{E_{(2)} A_c}. \tag{A.6}$$

It should be noted that the beam on the elastic foundation model, which is a similar simplified model and used to evaluate longitudinal bending deformation, overestimates the longitudinal axial stress of the lining because beam theory ignores the equilibrium of the force in the axial direction (Yasuda et al., 2018).

When the lining is finite and there are construction joints, a traction-free boundary condition is imposed as follows:

$$\left.\begin{aligned} \sigma_{zz,0(2s)}\,|_{z=z_1} &= E_{(2)} \frac{du_{z,0(2s)}}{dz}\Big|_{z=z_1} = 0 \\ \sigma_{zz,0(2s)}\,|_{z=z_2} &= E_{(2)} \frac{du_{z,0(2s)}}{dz}\Big|_{z=z_2} = 0 \end{aligned}\right\}, \tag{A.7}$$

where z_1 and z_2 are the position of both ends of the lining.

The solution satisfying Eq. (A.1) and Eq. (A.7) can be expressed as follows:

$$u_{z,0(2s)} = \frac{\lambda^2}{\gamma^2 + \lambda^2} U^i_{z,0(1)} e^{i(\gamma z - \omega t)} + A e^{\lambda z} + B e^{-\lambda z}, \tag{A.8}$$

where A and B are the coefficients calculated by the following equations:

$$\begin{pmatrix} A \\ B \end{pmatrix} = U^i_{z,0(1)} \frac{i\gamma\lambda}{\gamma^2 + \lambda^2} \begin{pmatrix} -e^{\lambda z_1} & e^{-\lambda z_1} \\ -e^{\lambda z_2} & e^{-\lambda z_2} \end{pmatrix}^{-1} \begin{pmatrix} e^{i(\gamma z_1 - \omega t)} \\ e^{i(\gamma z_2 - \omega t)} \end{pmatrix}. \tag{A.9}$$

References

Amorosi, A., Boldini, D., 2009. Numerical modelling of the transverse dynamic behaviour of circular tunnels in clayey soils. Soil Dynamics and Earthquake Engineering 29, 1059–1072.

Asakura, T., Sato, Y., 1996. Damage to mountain tunnels in hazard area. Soils and foundations , 301–310.

Chen, W., Shih, B., Chen, Y., Hung, J., Hwang, H., 2002. Seismic response of natural gas and water pipelines in the ji-ji earthquake. Soil Dynamics and Earthquake Engineering 22, 1209–1214.

Chen, Z., Shen, H., 2014. Dynamic centrifuge tests on isolation mechanism of tunnels subjected to seismic shaking. Tunnelling and Underground Space Technology 42, 67–77.

Fabozzi, S., Bilotta, E., Yu, H., Yuan, Y., 2018. Effects of the asynchronism of ground motion on the longitudinal behaviour of a circular tunnel. Tunnelling and Underground Space Technology 82, 529–541.

Flügge, W., 1973. Stress in Shells. Berlin and New York: Springer-Verlag.

Galler, R., Lorenz, S., 2018. Support elements in conventional tunneling–focus on long-term behavior. Underground Space 3, 277–287.

Hashash, Y., Hook, J., Schmidt, B., et al., 2001. Seismic design and analysis of underground structures. Tunnelling and Underground Space Technology 16, 247–293.

Hashash, Y., Park, D., Yao, J., et al., 2005. Ovaling deformations of circular tunnels under seismic loading, an update on seismic design and analysis of underground structures. Tunnelling and underground space technology 20, 435–441.

Kim, D., Konagai, K., 2000. Seismic isolation effect of a tunnel covered with coating material. Tunnelling and Underground Space Technology 15, 437–443.

Kiyomiya, O., 1995. Earthquake-resistant design features of immersed tunnels in japan. Tunnelling and Underground Space Technology 10, 463–475.

Kontoe, S., Zdravkovic, L., Potts, D.M., Menkiti, C.O., 2008. Case study on seismic tunnel response. Canadian Geotechnical Journal 45, 1743–1764.

Li, T., 2012. Damage to mountain tunnels related to the wenchuan earthquake and some suggestions for aseismic tunnel construction. Bulletin of Engineering Geology and the Environment 71, 297–308.

Miao, Y., Yao, E., Ruan, B., Zhuang, H., 2018. Seismic response of shield tunnel subjected to spatially varying earthquake ground motions. Tunnelling and Underground Space Technology 77, 216–226.

Mow, C., Pao, Y., 1971. The Diffraction of Elastic Waves and Dynamic Stress Concentrations. Rand Corporation.

O'Rourke, M.J., Liu, X., 1999. Response of buried pipelines subject to earthquake effects .

Sedarat, H., Kozak, A., Hashash, Y.M., Shamsabadi, A., Krimotat, A., 2009. Contact interface in seismic analysis of circular tunnels. Tunnelling and Underground Space Technology 24, 482–490.

Shi, P., 2015. Seismic wave propagation effects on buried segmented pipelines. Soil Dynamics and Earthquake Engineering 72, 89–98.

St John, C., Zahrah, T., 1987. Aseismic design of underground structures. Tunnelling and underground space technology 2, 165–197.

Stamos, A., Beskos, D., 1995. Dynamic analysis of large 3-d underground structures by the bem. Earthquake engineering & structural dynamics 24, 917–934.

Tianbin, L., 2008. Failure characteristics and influence factor analysis of mountain tunnels at epicenter zones of great wenchuan earthquake. Journal of Engineering Geology 16, 742–750.

Wang, W., Wang, T., Su, J., Lin, C., Seng, C., Huang, T., 2001. Assessment of damage in mountain tunnels due to the taiwan chi-chi earthquake. Tunnelling and underground space technology 16, 133–150.

Wang, Y., Shan, S., Zhang, C., Guo, P., 2019. Seismic response of tunnel lining structure in a thick expansive soil stratum. Tunnelling and Underground Space Technology 88, 250–259.

Wolf, J.P., 1985. Dynamic soil-structure interaction. Prentice-Hall Englewood Cliffs, New Jersey.

Yashiro, K., Kojima, Y., Shimizu, M., 2007. Historical earthquake damage to tunnels in japan and case studies of railway tunnels in the 2004 niigataken-chuetsu earthquake. Quarterly Report of RTRI 48, 136–141.

Yasuda, N., Tsukada, K., Asakura, T., 2014. Reconsideration of seismic deformation method for axial deformation on cylindrical underground structure (in japanese). Journal of Japan Society of Civil Engineers, Ser. A1 (Structural Engineering & Earthquake Engineering (SE/EE)) 70, 306–318.

Yasuda, N., Tsukada, K., Asakura, T., 2017. Elastic solutions for circular tunnel with void behind lining. Tunnelling and Underground Space Technology 70, 274–285.

Yasuda, N., Tsukada, K., Asakura, T., 2018. Reconsideration of seismic deformation method for longitudinal bending deformation of cylindrical underground structure (in japanese). Journal of Japan Society of Civil Engineers, Ser. A1 (Structural Engineering & Earthquake Engineering (SE/EE)) 74, 44–57.

Yasuda, N., Tsukada, K., Asakura, T., 2019. Three-dimensional seismic response of a cylindrical tunnel with voids behind the lining. Tunnelling and Underground Space Technology 84, 399–412.

Yu, H., Yuan, Y., Qiao, Z., Gu, Y., Yang, Z., Li, X., 2013. Seismic analysis of a long tunnel based on multi-scale method. Engineering Structures 49, 572–587.

Yu, H., Zhang, Z., Chen, J., Bobet, A., Zhao, M., Yuan, Y., 2018. Analytical solution for longitudinal seismic response of tunnel liners with sharp

stiffness transition. Tunnelling and Underground Space Technology 77, 103–114.

Zhang, X., Jiang, Y., Sugimoto, S., 2018. Seismic damage assessment of mountain tunnel: A case study on the tawarayama tunnel due to the 2016 kumamoto earthquake. Tunnelling and Underground Space Technology 71, 138 – 148.

Table A.1: Material properties.

Parameters	Ground	Structure
Young's modulus (GPa)	0.30	30
Poisson's ratio	0.30	0.20
Density (kg/m^3)	2000	2300
Radius (m)		5.0
Lining thickness (m)		0.30

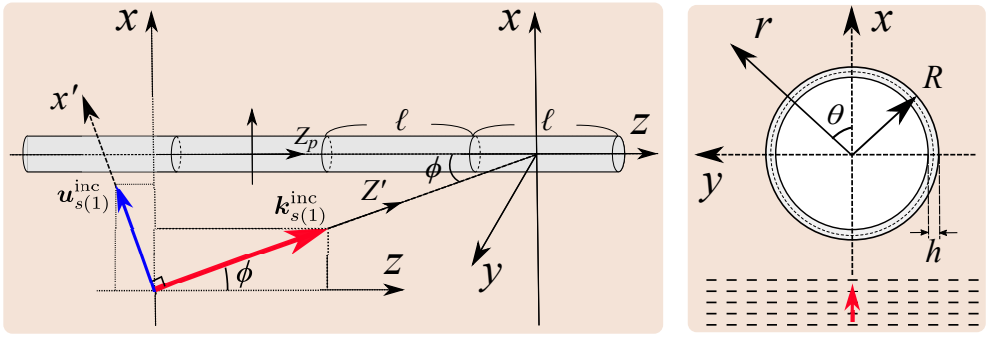

Figure A.1: A cylindrical tunnel with construction joints subjected to an obliquely incident plane harmonic shear wave.

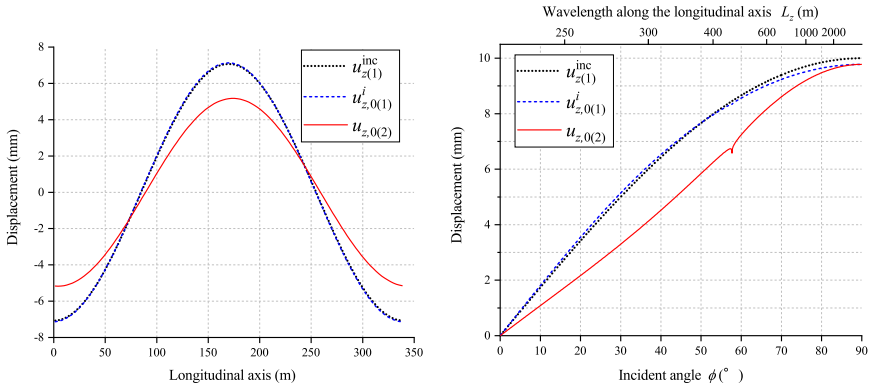

(a) (b)

Figure A.2: Longitudinal displacements at the ground-lining interface for the case without construction joints ($f = 1.0\,\text{Hz}$): (a) distributions at an incident angle of 45° and (b) amplitudes for various incident angles.

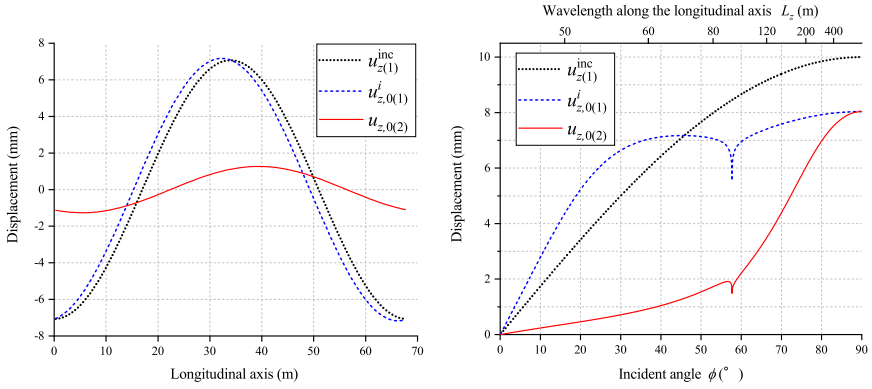

(a) (b)

Figure A.3: Longitudinal displacements at the ground-lining interface for the case without construction joints ($f = 5.0\,\text{Hz}$): (a) distributions at an incident angle of 45° and (b) amplitudes for various incident angles.

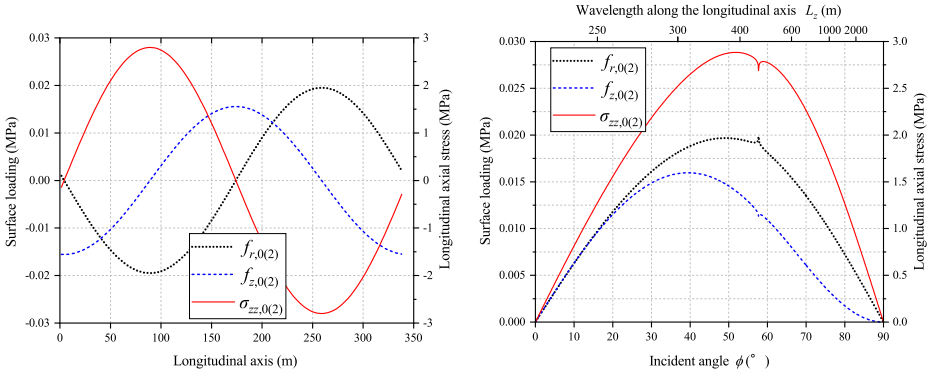

(a) (b)

Figure A.4: Surface loadings and longitudinal axial stress at the middle lining surface for the case without construction joints ($f = 1.0\,\mathrm{Hz}$): (a) distributions at an incident angle of 45° and (b) amplitudes for various incident angles.

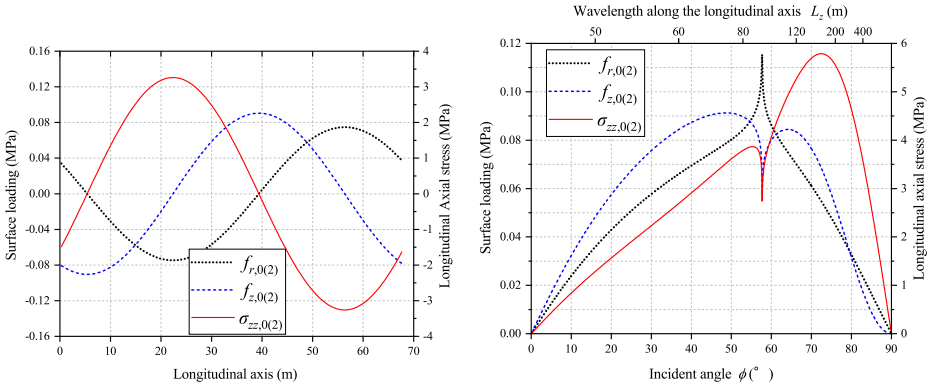

(a) (b)

Figure A.5: Surface loadings and longitudinal axial stress at the middle lining surface for the case without construction joints ($f = 5.0\,\mathrm{Hz}$): (a) distributions at an incident angle of 45° and (b) amplitudes for various incident angles.

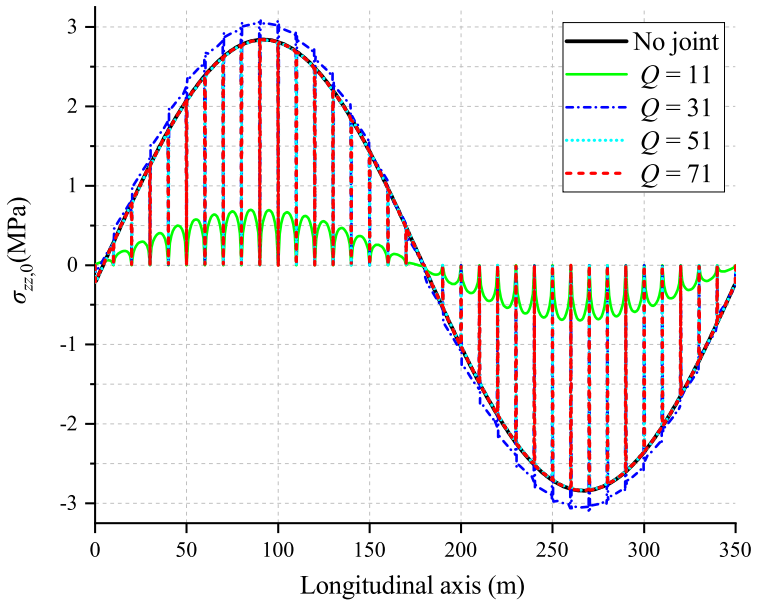

Figure A.6: Approximate solutions of longitudinal axial stress at the middle lining surface ($f = 1.0\,\mathrm{Hz}$). Q equidistant points were selected in every 10 m lining block for imposing the non-slip condition.

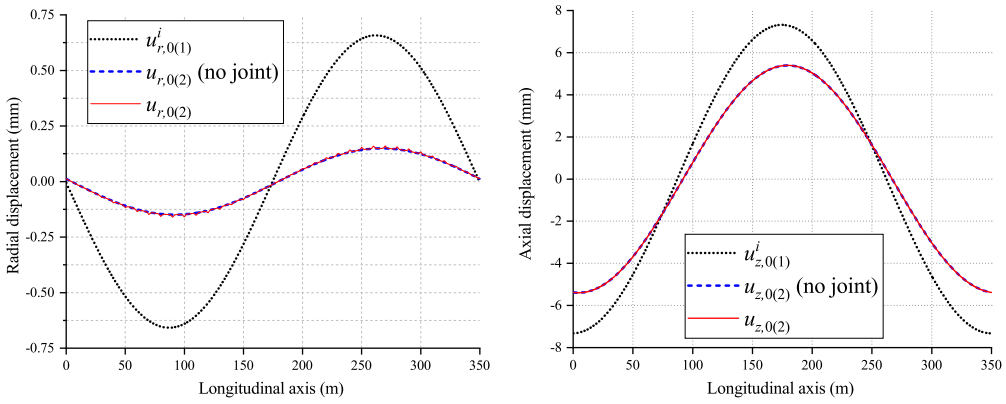

(a) (b)

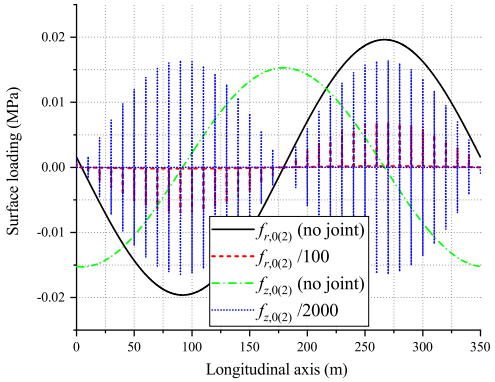

(c)

Figure A.7: Comparison of the solutions for the cases with and without construction joints ($f = 1.0\,\mathrm{Hz}$). For imposing the non-slip condition for the case with construction joints, 71 equidistant points were selected in every 10 m lining block: (a) radial displacement, (b) longitudinal displacement, and (c) surface loadings.

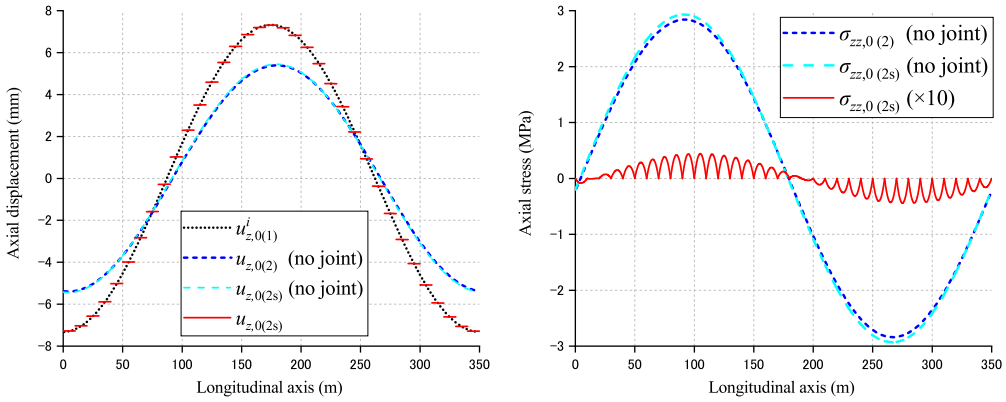

(a) (b)

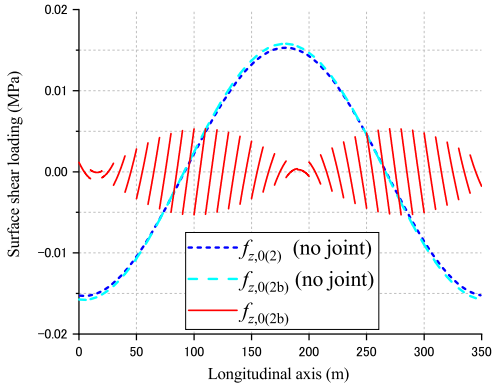

(c)

Figure A.8: Solutions derived from a simplified model assuming a constant ground stiffness ($f = 1.0\,\mathrm{Hz}$): (a) longitudinal displacement, (b) longitudinal axial stress, and (c) longitudinal surface shear loading.

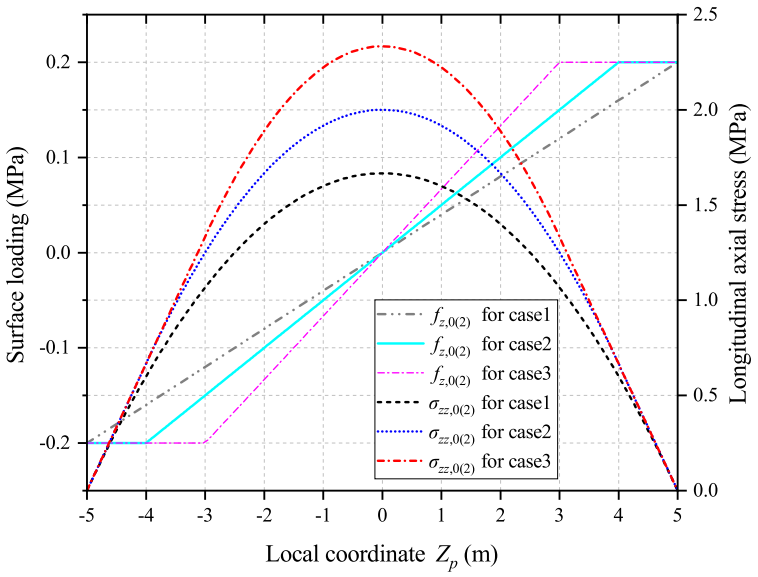

Figure A.9: Applied surface shear loading $f_{z,0(2)}$ and the resulting axial stress at the middle surfaces of the lining ($f_{r,0(2)} = 0$).